Cite as: L. De Marco *et al.*, *Science* 10.1126/science.aau7230 (2019).

A degenerate Fermi gas of polar molecules

Luigi De Marco[1,2], Giacomo Valtolina[1,2], Kyle Matsuda[1,2], William G. Tobias[1,2], Jacob P. Covey[1,2]*, Jun Ye[1,2]†

[1]JILA, National Institute of Standards and Technology (NIST) and University of Colorado, Boulder, CO 80309, USA. [2]Department of Physics, University of Colorado, 440 UCB, Boulder, CO 80309, USA.

***Present address: Department of Physics, California Institute of Technology, 1200 East California Blvd., Pasadena, CA 91125, USA.**

†Corresponding author. Email: ye@jila.colorado.edu

Experimental realization of a quantum degenerate gas of molecules would provide access to a wide range of phenomena in molecular and quantum sciences. However, the very complexity that makes ultracold molecules so enticing has made reaching degeneracy an outstanding experimental challenge over the past decade. We now report the production of a degenerate Fermi gas of ultracold polar molecules of potassium–rubidium (KRb). Through coherent adiabatic association in a deeply degenerate mixture of a rubidium Bose-Einstein condensate and a potassium Fermi gas, we produce molecules at temperatures below 0.3 times the Fermi temperature. We explore the properties of this reactive gas and demonstrate how degeneracy suppresses chemical reactions, making a long-lived degenerate gas of polar molecules a reality.

Ultracold polar molecules are ideal candidates to realize a plethora of proposals in molecular and many-body physics. These include the development of chemistry in the quantum regime (*1*), the emulation of strongly interacting lattice spin models (*2*–*6*), the production of topological phases in optical lattices (*7*–*10*), the exploration of fundamental symmetries (*11*–*15*), and the study of quantum information science (*16*–*18*). Although magnetic atoms also exhibit long-ranged dipolar interactions and can be used to carry out these proposals (*19*, *20*), polar molecules offer more tunable, stronger interactions and additional degrees of freedom. A low-entropy, quantum degenerate sample is a prerequisite for many of these explorations.

The intrinsic complexity of molecules relative to atoms, owing to the additional rotational and vibrational degrees of freedom, has made their cooling to ultralow temperatures one of the most significant experimental challenges in molecular physics (*21*). Although the direct laser cooling of certain diatomic molecules has progressed enormously in recent times so that magneto-optical (*22*–*25*) and pure optical (*26*) trapping have been demonstrated, phase space density in these systems remains many orders of magnitude away from degeneracy. To date, by far the coldest diatomic molecules have been made by cooling atoms to a few hundred nanokelvin (10^{-9} K) and coherently associating the ultracold atoms into deeply bound molecules using a Fano–Feshbach resonance (*27*) followed by stimulated Raman adiabatic passage (STIRAP) (*28*).

Thus far, KRb (*28*), NaK (*29*, *30*), RbCs (*31*, *32*), NaRb (*33*), and LiNa (*34*) have successfully been produced in deeply bound molecular states. Typically, such molecules can be produced in numbers ranging from hundreds to tens of thousands and at temperatures ranging from 250–600 nK. Reaching degeneracy in these experiments has been impeded by two major factors: the production of an adequate mixture of atoms to make a sufficient number of molecules, and rapid molecular loss. Challenges in producing a suitable mixture can be technical or physical, such as the immiscibility of two Bose-Einstein condensates (BECs) (*35*). Molecules can be lost owing to chemical reactions; for example, KRb undergoes the exothermic $2KRb \rightarrow K_2 + Rb_2$ reaction (*36*, *37*). Even molecules predicted to have endothermic reactions show large inelastic loss caused by the complex nature of the scattering process, which is still being investigated (*29*, *33*, *38*). Indeed, the lowest entropy samples of ground-state molecules have been produced in a three-dimensional optical lattice, where chemical reactions cannot occur, with an entropy of just 2.2 k_B per particle (*39*); however, producing quantum degenerate molecules in a bulk gas has so far been an outstanding experimental goal.

Here, we report the production of 10^5 fermionic $^{40}K^{87}Rb$ molecules at 250 nK and as many as 2.5×10^4 molecules at 50 nK, the latter corresponding to $T/T_F = 0.3$, where T_F is the Fermi temperature. Moreover, we observe that quantum degeneracy is accompanied by a suppression of chemical reactions.

The efficiency of ultracold molecule production is limited at low temperatures by rapid three-body recombination of the atomic species as well as the spatial mismatch between atomic density distributions (*40*–*42*). For KRb, however, in the limit where the K number vastly exceeds the Rb number, these effects can be mitigated, and the conversion to

molecules with respect to the minority species can be high (*42*). Furthermore, if the gases are deeply degenerate, the atoms' low entropy can be inherited by the molecules, resulting in a degenerate molecular gas (Fig. 1A). In our experiment, a large atom number before molecular association allowed us to take this approach, and afforded us the flexibility to produce KRb molecules over a wide range of temperatures, densities, and T/T_F.

After collecting ~10^9 ^{87}Rb atoms and 7×10^7 ^{40}K atoms in a vapor-cell magneto-optical trap, we cool the atoms to degeneracy by performing radiofrequency evaporation in an optically-plugged quadrupole trap followed by evaporation in a crossed optical dipole trap (xODT) (*43*). After optical evaporation is complete, the xODT is recompressed such that K experiences harmonic trapping frequencies of $(\omega_x, \omega_y, \omega_z) = 2\pi \times (45, 250, 80)$ Hz, with gravity along the y–direction. Trap frequencies are reduced by a factor of 0.72 and 0.79 for Rb and KRb, respectively, owing to differences in mass and AC polarizability. Slices through atomic column-integrated density distributions after 16 ms time of flight (TOF) for three representative conditions are shown in the upper row of Fig. 1B, and the corresponding numbers are given in Table 1. Among a number of technical improvements allowing us to produce a deeply degenerate mixture with a large number of atoms, a key advance has been the implementation of Λ–enhanced gray molasses on the D_1 ($4^2S_{1/2} \rightarrow 4^2P_{1/2}$) line of K (*44*) as well as the D_2 ($5^2S_{1/2} \rightarrow 5^2P_{3/2}$) line of Rb (*45*).

Ground state KRb molecules are produced by sweeping a magnetic field through an interspecies Fano–Feshbach resonance at B = 546.6 G to produce weakly bound Feshbach molecules (Fig. 1A) (*28*). The molecules are then coherently transferred to the ground state using STIRAP with ~90% efficiency. The experiments described here are conducted at zero electric field. The difference in trapping frequencies between molecules and atoms results in all three species having different equilibrium positions due to gravitational sag (*46*). Even though the molecules have the same initial temperature as the atoms, the initial non-equilibrium position sets the molecules in motion, and the gas rapidly heats up as potential energy is converted to kinetic energy. To mitigate this effect, prior to molecule production a one-dimensional optical lattice of 30 molecular recoil energies is turned on against gravity. This ensures that the molecules and atoms are at equilibrium at the same position in the corrugated potential. After molecules are produced, unpaired atoms are quickly blasted away with resonant light (*43*), the lattice is then ramped off in 5 ms, and no spatial oscillations or rapid heating are observed.

By varying the initial temperature and atomic number ratio, we generate molecular gases ranging from T/T_F greater than 1 to less than 0.3. Three representative conditions are summarized in Table 1, and slices through molecular column density distributions after 10 ms TOF are shown in the lower row of Fig. 1B; each molecular distribution shown is produced from the atomic conditions in the upper row of Fig. 1B. Over this range, the average molecular density varies from $0.5 - 2 \times 10^{12}$ cm^{-3}.

At low T/T_F, the effects of degeneracy on the molecular velocity distribution after TOF are clear. Two-dimensional absorption images are collected and fit (*43*); Fig. 2A shows the azimuthally-averaged density profile of a cloud of KRb molecules after 10 ms TOF. The profile is well fit by a Fermi–Dirac distribution (blue curve, $T/T_F = 0.31(2)$), whereas the classical Maxwell–Boltzmann distribution (red curve) overestimates the density at the center of the cloud and underestimates it in the wings. This is evident in the fit residuals, shown in the lower part of Fig. 2A, where the classical residuals exhibit ripples that are a hallmark of Fermi degeneracy (*47*). A Maxwell–Boltzmann fit to the wings of the profile (green curve), where the gas looks essentially classical, captures the temperature of the molecules but deviates at the center of the cloud.

The classical fit to the entire cloud systematically overestimates the temperature compared to the Fermi–Dirac fit because the Pauli exclusion principle prevents the multiple occupancy of low energy states. The difference between the temperatures measured with the two fits is a strong indicator of the degree of quantum degeneracy (*47*). Figure 2B shows the normalized difference between these, $\delta U/U_{Cl} = 1 - T/T_{Cl}$, for KRb as a function of T/T_F, where T_{Cl} is the temperature determined from the Maxwell–Boltzmann fit. As T/T_F is decreased, the normalized energy shows a deviation from the classical value, and for the most degenerate molecular clouds we currently produce, the deviation is larger than 30%. For comparison, the same quantity is shown for K at several values of T/T_F; both sets of data show good agreement with the theoretical prediction for an ideal Fermi gas (solid line).

Given the T/T_F measured for K prior to molecular association, we expect an increase in the molecular T/T_F by roughly a factor of 3–4 based on the change in particle number and trap frequency. However, we typically measure values of T/T_F that are only a factor of 2.5–3 larger than that of K. At values of $T/T_F \lesssim 0.1$ for K, 85% of the Rb is condensed, and the Rb to K ratio is made to be roughly 1:10 (Table 1, third row) in order to minimize three-body recombination during magnetoassociation (*42*, *48*). Under these conditions, molecules are produced with $T/T_F \lesssim 0.3$. Because the Rb BEC is fairly localized to the center of the K cloud (Fig. 1B), molecules are only produced in the lowest-entropy part of the Fermi sea (*49*), resulting in molecules that have a lower T/T_F than expected from uniform K conversion over the entire distribution. At such low temperatures, the conversion from Rb to Feshbach molecules can be as high as 50%, indicating that there is good local phase space overlap between potassium and the

rubidium condensate. In fact, because the density of the BEC is much higher than that of the K Fermi gas, the local conversion efficiency of K atoms approaches unity. This is the same principle of strong phase space matching that allowed for the efficient production of ground state molecules in a 3D optical lattice (*39*). In contrast, at high T/T_F, where we produce the largest absolute number of molecules, conversion is typically 15% of Rb (Table 1, first row).

Degenerate molecules are produced by adiabatically sweeping the magnetic field through a Fano–Feshbach resonance followed by coherent transfer to the ground state with high efficiency. Since the first step occurs on timescales that are comparable to the inverse trap frequency, the Feshbach molecules are produced at thermodynamic equilibrium (*50*). After transferring molecules to the ground state, we do not observe any large-scale spatial dynamics, suggesting that the ground-state molecular gas remains close to equilibrium. This is corroborated by the measured momentum distribution (Fig. 2A) and expansion energy (Fig. 2B). Furthermore, because inelastic collisions are predicted to be accompanied by a comparable number of elastic, momentum-exchanging collisions (*51*), this thermodynamic state is essentially maintained over the lifetime of the gas, as evidenced by the persistence of a low T/T_F, which grows slowly with time (Fig. S2B) (*43*). This is further supported by the dependence of chemical reactions on degeneracy, as described below.

Given that KRb molecules are fermions, intermolecular scattering must occur in the *p*-wave channel as this is the lowest energy antisymmetric collision channel. As such, the intermolecular potential (Fig. 3A) exhibits a centrifugal barrier through which molecules must tunnel in order to chemically react. According to the Bethe–Wigner threshold law (*52*, *53*), the tunneling rate (and therefore reaction rate), is proportional to the temperature, so that chemical reactions must slow down at low temperatures (*36*). Examples of density loss curves and their corresponding fits (see below) for two temperatures are shown in Fig. 3B. At low temperature, the density decays at a slower rate compared to at high temperature.

When a molecular collision leads to a reaction, the product molecules are ejected from the trap with high energy, leaving the remaining molecules unaffected as the mean free path is much larger than the size of the cloud. However, collisions tend to occur in the coldest, densest part of the cloud so that the lowest energy molecules react and are lost preferentially, leading to anti-evaporation and an overall heating of the cloud. We typically observe heating linear in time with rates ranging from h = 10–30 nK/s, slightly larger than a simple anti-evaporation model would suggest. However, this rate is small enough for the molecular T/T_F to remain close to its initial value over the course of the molecules' lifetime.

The reduction of density is determined by both the loss of KRb molecules and the increase in temperature. We fit our data to a simple two-body model that includes the effect of heating (*36*)

$$\frac{dn}{dt} = -\beta n^2 - \frac{3}{2}\frac{n}{T}\frac{dT}{dt} \quad (1)$$

where n is the average classical molecular density of the bulk gas; the temperature is a measured, linear function of time, $T = T_0 + ht$; and β is the two-body loss coefficient. Because two-particle threshold behavior predicts $\beta = bT$, the fitting of the data with Eq. 1 allows us to determine b (*43*).

Measurements of β as a function of initial molecular temperature are shown in Fig. 4A. Data points with a blue face correspond to $T/T_F \leq 0.6$ and those with a red face to $T/T_F > 0.6$; the solid red curve is the value predicted by multi-channel quantum defect theory (MQDT), based on a previously published ab initio calculation of the van der Waals coefficient, C_6 (*36*, *54*). The points with $T/T_F > 0.6$ follow the predicted MQDT trend closely, but those with $T/T_F \leq 0.6$ show deviations at all temperatures. Considering β/T, we observe a trend that is only dependent on T/T_F and not initial temperature. We find that at $T/T_F \leq 0.6$, β/T shows a strong deviation from the Bethe–Wigner threshold law, whereas above T/T_F = 0.6, β/T is constant, with a measured value of $\beta/T = 0.84(6) \times 10^{-5}$ cm^3 s^{-1} K^{-1} (black line in Fig. 4B, error range shown in gray). This value is in excellent agreement with the predicted MQDT value (*36*, *54*) of $\beta/T = 0.8(1) \times 10^{-5}$ cm^3 s^{-1} K^{-1} (red line in Fig. 4B). Our value is somewhat lower than the previously measured value of $\beta/T = 1.2(3) \times 10^{-5}$ cm^3 s^{-1} K^{-1} (*36*), with the discrepancy likely arising from the use of the corrugated potential to suppress gravitational sag in the current experiment.

Below $T/T_F = 0.6$, the measured β/T drops to values as low as $0.21(8) \times 10^{-5}$ cm^3 s^{-1} K^{-1}. A possible explanation for this observed deviation from a constant value is the change in density correlations as the gas becomes deeply degenerate. For a classical gas, the density sets the length scale of interparticle separation, which is much larger than the deBroglie wavelength, Λ. In this case, large density fluctuations occur on the molecular scale, and two particles can easily find a configuration to scatter in the *p*-wave channel. In a degenerate Fermi gas, however, the probability of finding two molecules within a short distance of each other decreases as T/T_F is lowered because of anti-bunching, with the average interparticle spacing being set by the deBroglie wavelength itself and ultimately by the Fermi wavevector, $2\pi/k_F$. This is the same physical phenomenon that gives rise to the Pauli pressure and reduced compressibility of a Fermi gas. This would cause an effective blockade that results in reduced density fluctuations (*55–57*) such that *p*-wave scattering and chemical reactions are suppressed beyond the Bethe–Wigner prediction. The suppressed collision rate manifests itself within our

model as a reduction in the measured β/T for the bulk gas, though the true two-body reaction rate constant is unaffected by degeneracy for any given molecular collision.

This effect is captured in the average relative number density fluctuation $\langle \delta n^2(\boldsymbol{r}) \rangle / \langle n(\boldsymbol{r}) \rangle$, which is shown as a blue line in Fig. 4B as a function of T/T_F. The curve is scaled to the MQDT value of β/T for $T/T_F > 1$, but otherwise has no fitting parameters. That this simple consideration qualitatively describes the change in reaction rate suggests that the reduced particle fluctuations correspondingly reduce the probability of two molecules colliding, resulting in a suppression of chemical reactions. Density fluctuations are most strongly suppressed in the center of the trap (*43*) where the majority of chemical reactions occur, which is a possible explanation for why some points fall below the expected fluctuation suppression curve. Similar suppression of loss caused by strong correlations has been observed in the three-body recombination rate of a one-dimensional Bose gas in which the particles have undergone fermionization (*58*). Furthermore, this effect is reminiscent of the reduction of the elastic *s*-wave collision rate observed in fermionic atoms (*59*, *60*); however, in the elastic case, the reduction of the elastic cross section is attributed to the unavailability of empty states to scatter into, which is not relevant for inelastic collisions.

Although the qualitative agreement between the data and the suppression of density fluctuations is suggestive, a complete theory must treat the many-body nature of the degenerate gas within which the chemical reactions are taking place. . In particular, it is important to consider the degree to which molecules thermalize after some are lost to chemical reactions. Furthermore, as T/T_F is decreased well below 0.3, collisions will be dominated by molecules near the Fermi surface so that the mean relative collision energy will deviate from the classical equipartition value to the quantum value of $\frac{3}{4}k_B T_F$ per particle.

The production of a degenerate Fermi gas of dipolar molecules opens previously unexplored paths in ultracold molecular science. In a bulk gas, we now have the opportunity to study chemical reactions in a regime where quantum degeneracy and quantum fluctuations compete with classical chemical reaction dynamics. Furthermore, this work shows great promise for the exploration of degenerate molecules in electric fields, where the strong dipole–dipole interaction dominates. In this limit, we expect to see interaction-induced effects such as the deformation of the Fermi surface and the development of exotic many-body correlations.

REFERENCES AND NOTES

1. L. D. Carr, D. DeMille, R. V. Krems, J. Ye, Cold and ultracold molecules: Science, technology and applications. *New J. Phys.* **11**, 055049 (2009). doi:10.1088/1367-2630/11/5/055049
2. A. Micheli, G. K. Brennen, P. Zoller, A toolbox for lattice-spin models with polar molecules. *Nat. Phys.* **2**, 341–347 (2006). doi:10.1038/nphys287
3. K. Osterloh, N. Barberán, M. Lewenstein, Strongly correlated states of ultracold rotating dipolar Fermi gases. *Phys. Rev. Lett.* **99**, 160403 (2007). doi:10.1103/PhysRevLett.99.160403 Medline
4. H. P. Büchler, E. Demler, M. Lukin, A. Micheli, N. Prokof'ev, G. Pupillo, P. Zoller, Strongly correlated 2D quantum phases with cold polar molecules: Controlling the shape of the interaction potential. *Phys. Rev. Lett.* **98**, 060404 (2007). doi:10.1103/PhysRevLett.98.060404 Medline
5. A. V. Gorshkov, S. R. Manmana, G. Chen, J. Ye, E. Demler, M. D. Lukin, A. M. Rey, Tunable superfluidity and quantum magnetism with ultracold polar molecules. *Phys. Rev. Lett.* **107**, 115301 (2011). doi:10.1103/PhysRevLett.107.115301 Medline
6. M. A. Baranov, M. Dalmonte, G. Pupillo, P. Zoller, Condensed matter theory of dipolar quantum gases. *Chem. Rev.* **112**, 5012–5061 (2012). doi:10.1021/cr2003568 Medline
7. N. R. Cooper, G. V. Shlyapnikov, Stable topological superfluid phase of ultracold polar fermionic molecules. *Phys. Rev. Lett.* **103**, 155302 (2009). doi:10.1103/PhysRevLett.103.155302 Medline
8. N. Y. Yao, A. V. Gorshkov, C. R. Laumann, A. M. Läuchli, J. Ye, M. D. Lukin, Realizing fractional Chern insulators in dipolar spin systems. *Phys. Rev. Lett.* **110**, 185302 (2013). doi:10.1103/PhysRevLett.110.185302 Medline
9. S. V. Syzranov, M. L. Wall, V. Gurarie, A. M. Rey, Spin-orbital dynamics in a system of polar molecules. *Nat. Commun.* **5**, 5391 (2014). doi:10.1038/ncomms6391 Medline
10. D. Peter, N. Y. Yao, N. Lang, S. D. Huber, M. D. Lukin, H. P. Büchler, Topological bands with a Chern number C = 2 by dipolar exchange interactions. *Phys. Rev. A* **91**, 053617 (2015). doi:10.1103/PhysRevA.91.053617
11. M. G. Kozlov, L. N. Labzowsky, Parity violation effects in diatomics. *J. Phys. B* **28**, 1933–1961 (1995). doi:10.1088/0953-4075/28/10/008
12. V. V. Flambaum, M. G. Kozlov, Enhanced sensitivity to the time variation of the fine-structure constant and mp/me in diatomic molecules. *Phys. Rev. Lett.* **99**, 150801 (2007). doi:10.1103/PhysRevLett.99.150801 Medline
13. J. J. Hudson, D. M. Kara, I. J. Smallman, B. E. Sauer, M. R. Tarbutt, E. A. Hinds, Improved measurement of the shape of the electron. *Nature* **473**, 493–496 (2011). doi:10.1038/nature10104 Medline
14. J. Baron, W. C. Campbell, D. DeMille, J. M. Doyle, G. Gabrielse, Y. V. Gurevich, P. W. Hess, N. R. Hutzler, E. Kirilov, I. Kozyryev, B. R. O'Leary, C. D. Panda, M. F. Parsons, E. S. Petrik, B. Spaun, A. C. Vutha, A. D. West; ACME Collaboration, Order of magnitude smaller limit on the electric dipole moment of the electron. *Science* **343**, 269–272 (2014). doi:10.1126/science.1248213 Medline
15. W. B. Cairncross, D. N. Gresh, M. Grau, K. C. Cossel, T. S. Roussy, Y. Ni, Y. Zhou, J. Ye, E. A. Cornell, Precision Measurement of the Electron's Electric Dipole Moment Using Trapped Molecular Ions. *Phys. Rev. Lett.* **119**, 153001 (2017). doi:10.1103/PhysRevLett.119.153001 Medline
16. A. André, D. DeMille, J. M. Doyle, M. D. Lukin, S. E. Maxwell, P. Rabl, R. J. Schoelkopf, P. Zoller, A coherent all-electrical interface between polar molecules and mesoscopic superconducting resonators. *Nat. Phys.* **2**, 636–642 (2006). doi:10.1038/nphys386
17. S. F. Yelin, K. Kirby, R. Côté, Schemes for robust quantum computation with polar molecules. *Phys. Rev. A* **74**, 050301 (2006). doi:10.1103/PhysRevA.74.050301
18. K.-K. Ni, T. Rosenband, D. D. Grimes, Dipolar exchange quantum logic gate with polar molecules. *Chem. Sci.* **9**, 6830–6838 (2018). doi:10.1039/C8SC02355G Medline
19. T. Lahaye, C. Menotti, L. Santos, M. Lewenstein, T. Pfau, The physics of dipolar bosonic quantum gases. *Rep. Prog. Phys.* **72**, 126401 (2009). doi:10.1088/0034-4885/72/12/126401
20. K. Aikawa, A. Frisch, M. Mark, S. Baier, R. Grimm, F. Ferlaino, Reaching Fermi degeneracy via universal dipolar scattering. *Phys. Rev. Lett.* **112**, 010404 (2014). doi:10.1103/PhysRevLett.112.010404 Medline

21. J. L. Bohn, A. M. Rey, J. Ye, Cold molecules: Progress in quantum engineering of chemistry and quantum matter. *Science* **357**, 1002–1010 (2017). doi:10.1126/science.aam6299 Medline
22. M. T. Hummon, M. Yeo, B. K. Stuhl, A. L. Collopy, Y. Xia, J. Ye, 2D Magneto-optical trapping of diatomic molecules. *Phys. Rev. Lett.* **110**, 143001 (2013). doi:10.1103/PhysRevLett.110.143001 Medline
23. J. F. Barry, D. J. McCarron, E. B. Norrgard, M. H. Steinecker, D. DeMille, Magneto-optical trapping of a diatomic molecule. *Nature* **512**, 286–289 (2014). doi:10.1038/nature13634 Medline
24. L. Anderegg, B. L. Augenbraun, E. Chae, B. Hemmerling, N. R. Hutzler, A. Ravi, A. Collopy, J. Ye, W. Ketterle, J. M. Doyle, Radio Frequency Magneto-Optical Trapping of CaF with High Density. *Phys. Rev. Lett.* **119**, 103201 (2017). doi:10.1103/PhysRevLett.119.103201 Medline
25. S. Truppe, H. J. Williams, M. Hambach, L. Caldwell, N. J. Fitch, E. A. Hinds, B. E. Sauer, M. R. Tarbutt, Molecules cooled below the Doppler limit. *Nat. Phys.* **13**, 1173–1176 (2017). doi:10.1038/nphys4241
26. L. Anderegg, B. L. Augenbraun, Y. Bao, S. Burchesky, L. W. Cheuk, W. Ketterle, J. M. Doyle, Laser cooling of optically trapped molecules. *Nat. Phys.* **14**, 890–893 (2018). doi:10.1038/s41567-018-0191-z
27. C. Chin, R. Grimm, P. Julienne, E. Tiesinga, Feshbach resonances in ultracold gases. *Rev. Mod. Phys.* **82**, 1225–1286 (2010). doi:10.1103/RevModPhys.82.1225
28. K. K. Ni, S. Ospelkaus, M. H. G. de Miranda, A. Pe'er, B. Neyenhuis, J. J. Zirbel, S. Kotochigova, P. S. Julienne, D. S. Jin, J. Ye, A high phase-space-density gas of polar molecules. *Science* **322**, 231–235 (2008). doi:10.1126/science.1163861 Medline
29. J. W. Park, S. A. Will, M. W. Zwierlein, Ultracold Dipolar Gas of Fermionic 23Na40 K Molecules in Their Absolute Ground State. *Phys. Rev. Lett.* **114**, 205302 (2015). doi:10.1103/PhysRevLett.114.205302 Medline
30. F. Seeßelberg, N. Buchheim, Z.-K. Lu, T. Schneider, X.-Y. Luo, E. Tiemann, I. Bloch, C. Gohle, Modeling the adiabatic creation of ultracold polar 23 Na 40 K molecules. *Phys. Rev. A (Coll. Park)* **97**, 013405 (2018). doi:10.1103/PhysRevA.97.013405
31. T. Takekoshi, L. Reichsöllner, A. Schindewolf, J. M. Hutson, C. R. Le Sueur, O. Dulieu, F. Ferlaino, R. Grimm, H.-C. Nägerl, Ultracold dense samples of dipolar RbCs molecules in the rovibrational and hyperfine ground state. *Phys. Rev. Lett.* **113**, 205301 (2014). doi:10.1103/PhysRevLett.113.205301 Medline
32. P. K. Molony, P. D. Gregory, Z. Ji, B. Lu, M. P. Köppinger, C. R. Le Sueur, C. L. Blackley, J. M. Hutson, S. L. Cornish, Creation of ultracold $^{87}Rb^{133}Cs$ molecules in the rovibrational ground state. *Phys. Rev. Lett.* **113**, 255301 (2014). doi:10.1103/PhysRevLett.113.255301 Medline
33. M. Guo, B. Zhu, B. Lu, X. Ye, F. Wang, R. Vexiau, N. Bouloufa-Maafa, G. Quéméner, O. Dulieu, D. Wang, Creation of an Ultracold Gas of Ground-State Dipolar ^23Na^87Rb Molecules. *Phys. Rev. Lett.* **116**, 205303 (2016). doi:10.1103/PhysRevLett.116.205303 Medline
34. T. M. Rvachov, H. Son, A. T. Sommer, S. Ebadi, J. J. Park, M. W. Zwierlein, W. Ketterle, A. O. Jamison, Long-Lived Ultracold Molecules with Electric and Magnetic Dipole Moments. *Phys. Rev. Lett.* **119**, 143001 (2017). doi:10.1103/PhysRevLett.119.143001 Medline
35. L. Reichsöllner, A. Schindewolf, T. Takekoshi, R. Grimm, H.-C. Nägerl, Quantum Engineering of a Low-Entropy Gas of Heteronuclear Bosonic Molecules in an Optical Lattice. *Phys. Rev. Lett.* **118**, 073201 (2017). doi:10.1103/PhysRevLett.118.073201 Medline
36. S. Ospelkaus, K.-K. Ni, D. Wang, M. H. G. de Miranda, B. Neyenhuis, G. Quéméner, P. S. Julienne, J. L. Bohn, D. S. Jin, J. Ye, Quantum-state controlled chemical reactions of ultracold potassium-rubidium molecules. *Science* **327**, 853–857 (2010). doi:10.1126/science.1184121 Medline
37. K. K. Ni, S. Ospelkaus, D. Wang, G. Quéméner, B. Neyenhuis, M. H. G. de Miranda, J. L. Bohn, J. Ye, D. S. Jin, Dipolar collisions of polar molecules in the quantum regime. *Nature* **464**, 1324–1328 (2010). doi:10.1038/nature08953 Medline
38. M. Mayle, G. Quéméner, B. P. Ruzic, J. L. Bohn, Scattering of ultracold molecules in the highly resonant regime. *Phys. Rev. A* **87**, 012709 (2013). doi:10.1103/PhysRevA.87.012709
39. S. A. Moses, J. P. Covey, M. T. Miecnikowski, B. Yan, B. Gadway, J. Ye, D. S. Jin, Creation of a low-entropy quantum gas of polar molecules in an optical lattice. *Science* **350**, 659–662 (2015). doi:10.1126/science.aac6400 Medline
40. J. Herbig, T. Kraemer, M. Mark, T. Weber, C. Chin, H. C. Nägerl, R. Grimm, Preparation of a pure molecular quantum gas. *Science* **301**, 1510–1513 (2003). doi:10.1126/science.1088876 Medline
41. J. J. Zirbel, K.-K. Ni, S. Ospelkaus, T. L. Nicholson, M. L. Olsen, P. S. Julienne, C. E. Wieman, J. Ye, D. S. Jin, Heteronuclear molecules in an optical dipole trap. *Phys. Rev. A* **78**, 013416 (2008). doi:10.1103/PhysRevA.78.013416
42. T. D. Cumby, R. A. Shewmon, M.-G. Hu, J. D. Perreault, D. S. Jin, Feshbach-molecule formation in a Bose-Fermi mixture. *Phys. Rev. A* **87**, 012703 (2013). doi:10.1103/PhysRevA.87.012703
43. Materials and methods are available as supplementary materials.
44. D. Rio Fernandes, F. Sievers, N. Kretzschmar, S. Wu, C. Salomon, F. Chevy, Sub-Doppler laser cooling of fermionic ^{40} K atoms in three-dimensional gray optical molasses. *Europhys. Lett.* **100**, 63001 (2012). doi:10.1209/0295-5075/100/63001
45. S. Rosi, A. Burchianti, S. Conclave, D. S. Naik, G. Roati, C. Fort, F. Minardi, Λ-enhanced grey molasses on the D_2 transition of Rubidium-87 atoms. *Sci. Rep.* **8**, 1301 (2018). doi:10.1038/s41598-018-19814-z Medline
46. G. Delannoy, S. G. Murdoch, V. Boyer, V. Josse, P. Bouyer, A. Aspect, Understanding the production of dual Bose-Einstein condensation with sympathetic cooling. *Phys. Rev. A* **63**, 051602 (2001). doi:10.1103/PhysRevA.63.051602
47. B. DeMarco, D. S. Jin, Onset of fermi degeneracy in a trapped atomic Gas. *Science* **285**, 1703–1706 (1999). doi:10.1126/science.285.5434.1703 Medline
48. J. J. Zirbel, K.-K. Ni, S. Ospelkaus, J. P. D'Incao, C. E. Wieman, J. Ye, D. S. Jin, Collisional stability of fermionic Feshbach molecules. *Phys. Rev. Lett.* **100**, 143201 (2008). doi:10.1103/PhysRevLett.100.143201 Medline
49. T.-L. Ho, Q. Zhou, Squeezing out the entropy of fermions in optical lattices. *Proc. Natl. Acad. Sci. U.S.A.* **106**, 6916–6920 (2009). doi:10.1073/pnas.0809862105 Medline
50. M. Greiner, C. A. Regal, D. S. Jin, Emergence of a molecular Bose-Einstein condensate from a Fermi gas. *Nature* **426**, 537–540 (2003). doi:10.1038/nature02199 Medline
51. Z. Idziaszek, G. Quéméner, J. L. Bohn, P. S. Julienne, Simple quantum model of ultracold polar molecule collisions. *Phys. Rev. A* **82**, 020703 (2010). doi:10.1103/PhysRevA.82.020703
52. E. P. Wigner, On the Behavior of Cross Sections Near Thresholds. *Phys. Rev.* **73**, 1002–1009 (1948). doi:10.1103/PhysRev.73.1002
53. H. R. Sadeghpour, J. L. Bohn, M. J. Cavagnero, B. D. Esry, I. I. Fabrikant, J. H. Macek, A. R. P. Rau, Collisions near threshold in atomic and molecular physics. *J. Phys. B* **33**, R93–R140 (2000). doi:10.1088/0953-4075/33/5/201
54. Z. Idziaszek, P. S. Julienne, Universal rate constants for reactive collisions of ultracold molecules. *Phys. Rev. Lett.* **104**, 113202 (2010). doi:10.1103/PhysRevLett.104.113202 Medline
55. T. Rom, T. Best, D. van Oosten, U. Schneider, S. Fölling, B. Paredes, I. Bloch, Free fermion antibunching in a degenerate atomic Fermi gas released from an optical lattice. *Nature* **444**, 733–736 (2006). doi:10.1038/nature05319 Medline
56. C. Sanner, E. J. Su, A. Keshet, R. Gommers, Y. I. Shin, W. Huang, W. Ketterle, Suppression of density fluctuations in a quantum degenerate Fermi gas. *Phys. Rev. Lett.* **105**, 040402 (2010). doi:10.1103/PhysRevLett.105.040402 Medline
57. T. Müller, B. Zimmermann, J. Meineke, J.-P. Brantut, T. Esslinger, H. Moritz, Local observation of antibunching in a trapped Fermi gas. *Phys. Rev. Lett.* **105**, 040401 (2010). doi:10.1103/PhysRevLett.105.040401 Medline
58. B. Laburthe Tolra, K. M. O'Hara, J. H. Huckans, W. D. Phillips, S. L. Rolston, J. V. Porto, Observation of reduced three-body recombination in a correlated 1D degenerate Bose gas. *Phys. Rev. Lett.* **92**, 190401 (2004). doi:10.1103/PhysRevLett.92.190401 Medline
59. B. DeMarco, S. B. Papp, D. S. Jin, Pauli blocking of collisions in a quantum degenerate atomic Fermi gas. *Phys. Rev. Lett.* **86**, 5409–5412 (2001). doi:10.1103/PhysRevLett.86.5409 Medline
60. K. Aikawa, A. Frisch, M. Mark, S. Baier, R. Grimm, J. L. Bohn, D. S. Jin, G. M. Bruun, F. Ferlaino, Anisotropic relaxation dynamics in a dipolar Fermi gas driven out of equilibrium. *Phys. Rev. Lett.* **113**, 263201 (2014). doi:10.1103/PhysRevLett.113.263201 Medline
61. L. De Marco *et al.*, Replication Data for: A Degenerate Fermi Gas of Polar Molecules. Harvard Dataverse, version 1.0 (2019); doi:10.7910/DVN/RLOBHV

ACKNOWLEDGMENTS

We dedicate this work to the memory of Deborah Jin, whose brilliance and passion inspire us all. We thank J. Bohn, E. Cornell, C. Greene, Peiru He, M. Holland, S. Moses, and A. M. Rey for useful discussions. **Funding:** This work is supported by NIST, AFOSR-MURI, ARO-MURI, and the NSF JILA Physics Frontier Center (NSF PHY-1734006). **Author contributions:** All authors contributed to carrying out the experiments, interpreting the results, and writing the manuscript. **Competing interests:** The authors declare that they have no competing financial interests. **Data and materials availability:** Data from the main text and supplementary materials are available through the Harvard Dataverse at (*61*).

SUPPLEMENTARY MATERIALS

www.sciencemag.org/cgi/content/full/science.aau7230/DC1
Materials and Methods
Figs. S1 to S3

9 July 2018; accepted 4 January 2019
Published online 17 January 2019
10.1126/science.aau7230

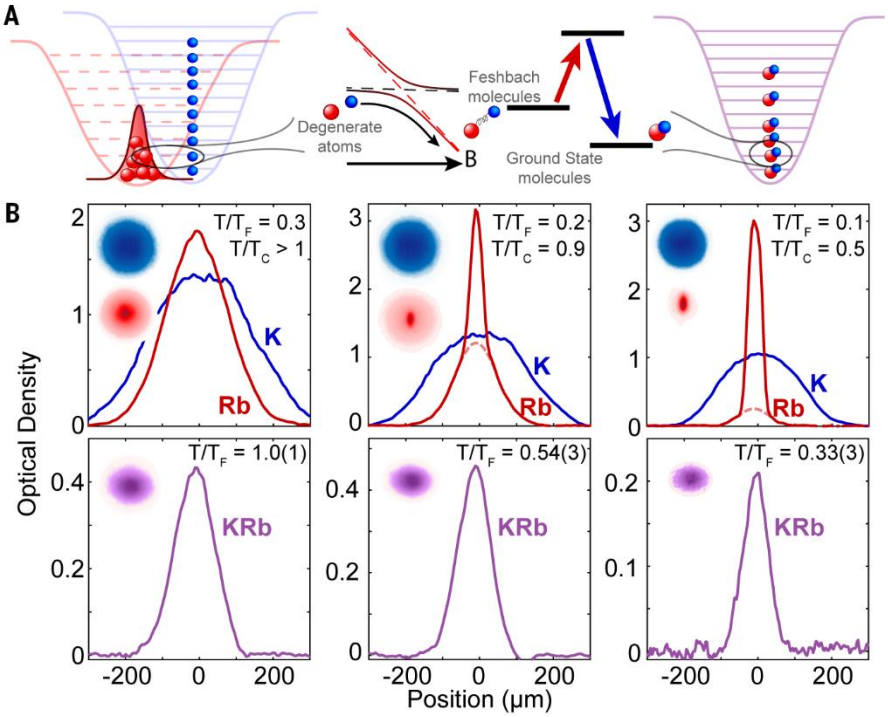

Fig. 1. Fig. 1. Production of degenerate molecules. (A) Beginning with degenerate gases of Rb (red) and K (blue), Feshbach molecules are created by sweeping a magnetic field through a Fano–Feshbach resonance. The weakly bound molecules are coherently transferred to the ground state using STIRAP. The resulting molecules reflect the degeneracy of their parent atoms. (B) Slices through images of atomic mixtures (2 averages, 16 ms TOF, upper row) and ground state molecules (4 averages, 10 ms TOF, lower row) for molecular T/T_F ranging from 0.3 to 1 (right to left). Inset images show false-color 2D column density, with blue corresponding to K and red to Rb. Dashed red lines correspond to non-condensed component of Rb cloud. The TOF images reflect the differing momentum distributions of the atoms and molecules.

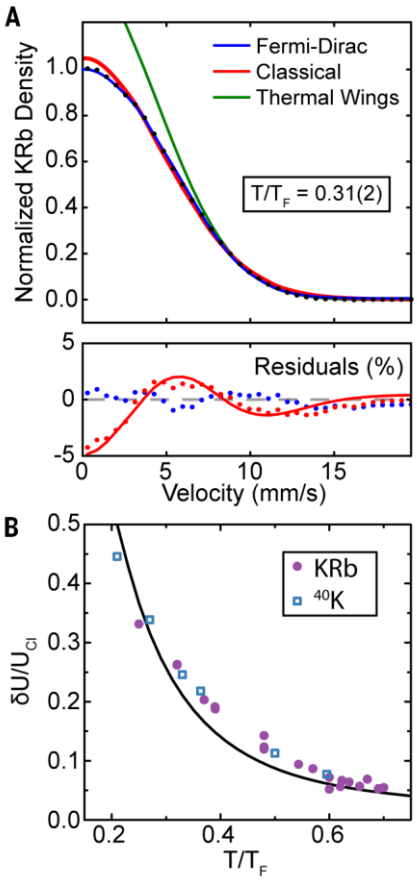

Fig. 2. Signatures of quantum degeneracy. (A) An azimuthally-averaged molecular density profile with $T/T_F = 0.31(2)$ fit to a Fermi–Dirac distribution (blue curve) and a classical Maxwell-Boltzmann distribution (red curve). The fit residuals (lower panel) show the deviation of the classical fit (red points) characteristic of degeneracy; the solid curve corresponds to the difference of the residuals. Fitting only the wings of the cloud to a Maxwell–Boltzmann distribution (green curve) accurately captures the temperature but overestimates the density in the center. (B) The deviation of the internal energy of the molecular gas from its classical value grows as T/T_F is reduced. The solid curve is the expected result for an ideal Fermi gas, and the results for K are shown for comparison.

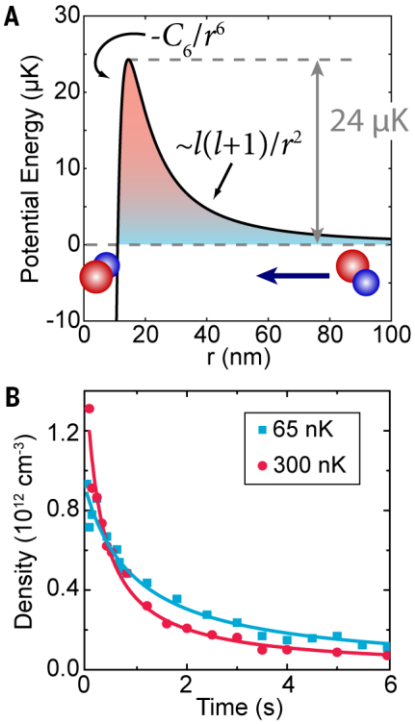

Fig. 3. Intermolecular reactions. (**A**) The intermolecular *p*-wave (l = 1) scattering potential for KRb (*36*); molecules can react once they have tunneled through the barrier. (**B**) As reactions occur, molecular density (shown at two temperatures) decays according to a two-body rate law. The rate constant decreases with decreasing temperature in accordance with the Bethe–Wigner threshold law (see text).

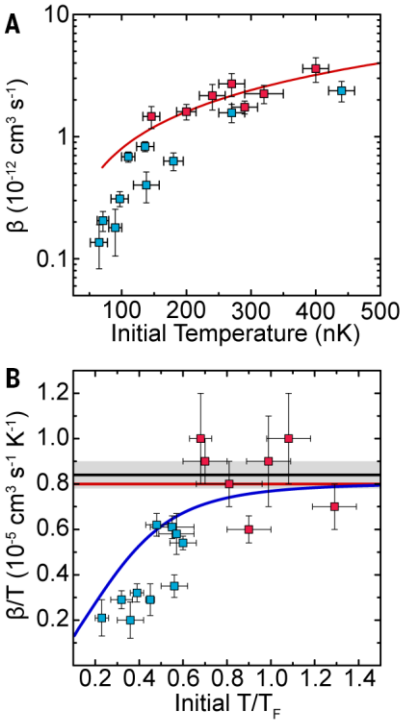

Fig. 4. Temperature dependence of reaction rate constants. (A) The reaction rate constant β for initial temperatures ranging from $T = 70 – 450$ nK. Blue-filled points correspond to $T/T_F \leq 0.6$ and red-filled points to $T/T_F > 0.6$. The red curve is the value expected from MQDT. (B) Temperature-normalized reaction rate constants from (A) as a function of degeneracy. The measured β/T, as determined by fitting the average density to the solution of Eq. 1, appears to decrease sharply when $T/T_F < 0.6$ owing to the suppression of fluctuations. The solid black line and gray bar are the average β/T for $T/T_F > 0.6$ and corresponding error range. The red line is the MQDT value and the blue curve is the average relative density fluctuations.

Table 1. Atom and molecule conditions corresponding to Fig. 1B.

T (nK)	Rb Number	T/T_c	K Number	T/T_F	KRb Number	T/T_F
230	6×10^5	> 1	1.2×10^6	0.3	$1.0(1) \times 10^5$	1.0(1)
110	2×10^5	0.9	1×10^6	0.2	$5.0(5) \times 10^4$	0.54(3)
50	7×10^4	0.5	5×10^5	0.1	$3.0(5) \times 10^4$	0.33(3)

A degenerate Fermi gas of polar molecules

Luigi De Marco, Giacomo Valtolina, Kyle Matsuda, William G. Tobias, Jacob P. Covey and Jun Ye

published online January 17, 2019

Science (print ISSN 0036-8075; online ISSN 1095-9203) is published by the American Association for the Advancement of Science, 1200 New York Avenue NW, Washington, DC 20005.